Journal of Cerebral Blood Flow & Metabolism (2015) 35, 1213–1219

www.jcbfm.com

ORIGINAL ARTICLE

Eccentricity mapping of the human visual cortex to evaluate temporal dynamics of functional $T_{1\rho}$ mapping

Hye-Young Heo[1,2], John A Wemmie[3,4,5], Casey P Johnson[1], Daniel R Thedens[1] and Vincent A Magnotta[1,2,3]

Recent experiments suggest that T_1 relaxation in the rotating frame ($T_{1\rho}$) is sensitive to metabolism and can detect localized activity-dependent changes in the human visual cortex. Current functional magnetic resonance imaging (fMRI) methods have poor temporal resolution due to delays in the hemodynamic response resulting from neurovascular coupling. Because $T_{1\rho}$ is sensitive to factors that can be derived from tissue metabolism, such as pH and glucose concentration via proton exchange, we hypothesized that activity-evoked $T_{1\rho}$ changes in visual cortex may occur before the hemodynamic response measured by blood oxygenation level-dependent (BOLD) and arterial spin labeling (ASL) contrast. To test this hypothesis, functional imaging was performed using $T_{1\rho}$, BOLD, and ASL in human participants viewing an expanding ring stimulus. We calculated eccentricity phase maps across the occipital cortex for each functional signal and compared the temporal dynamics of $T_{1\rho}$ versus BOLD and ASL. The results suggest that $T_{1\rho}$ changes precede changes in the two blood flow-dependent measures. These observations indicate that $T_{1\rho}$ detects a signal distinct from traditional fMRI contrast methods. In addition, these findings support previous evidence that $T_{1\rho}$ is sensitive to factors other than blood flow, volume, or oxygenation. Furthermore, they suggest that tissue metabolism may be driving activity-evoked $T_{1\rho}$ changes.

Journal of Cerebral Blood Flow & Metabolism (2015) **35,** 1213–1219; doi:10.1038/jcbfm.2015.94; published online 13 May 2015

Keywords: ASL; BOLD; Eccentricity Mapping; Functional MRI; $T_{1\rho}$

INTRODUCTION

Assessment of brain function in humans has largely utilized functional imaging approaches that are based on blood flow changes resulting from increased neuronal metabolism. The most common imaging modalities used to noninvasively study brain function include[15] O-water positron emission tomography, functional magnetic resonance imaging (fMRI), and functional near-infrared spectroscopy. The most common tool used to study brain function is the blood oxygenation level-dependent (BOLD) fMRI technique. The BOLD technique is dependent on changes in the relative amount of deoxygenated versus oxygenated hemoglobin that occurs in the venous system downstream of the activation site.[1,2] In addition, the vascular dilation that occurs in response to increased metabolic demands occurs several millimeters upstream of the activation site and feeds a vascular territory larger than the local area of activation. The aforementioned effects result in a loss of spatial resolution for BOLD imaging.[3] The use of the blood flow response to assess brain function also reduces the temporal resolution of the imaging technique. The hemodynamic response to neural activity is delayed by approximately 3 to 5 seconds from the onset of neural activation and does not reach its peak until 5 to 10 seconds after stimulus onset.[4,5] To overcome some of these limitations, other fMRI techniques have been proposed including arterial spin labeling (ASL)[6] and vascular space occupancy.[7,8] The ASL signal originates predominantly from tissue and capillaries,[6,9] which provides more localization of the activation area. However, ASL imaging depends on the hemodynamic response resulting from neurovascular coupling.[10] Arterial spin labeling has been shown to occur faster than the BOLD response[10] because it is measured in the arterial system versus the venous system, but it still significantly lags brain activity. Vascular space occupancy is an imaging technique that measures cerebral blood volume and has been shown to be more specific to the region of activation as compared with BOLD.[7,11] There have been findings showing both a fast and a slow component of the cerebral blood volume response.[12–14]

Functional imaging techniques that are sensitive to metabolite concentrations will likely generate a faster response and be more specific to the area of activation than techniques sensitive to blood flow changes. Importantly, the activity-evoked changes in metabolites and pH as well as other molecules including nitric oxide, potassium, O_2, and adenosine[15] have been suggested to precede and help signal the need for increased blood flow to meet increased tissue demand for nutrients and waste removal. Accumulating evidence suggests that brain activity alters local metabolite concentrations sufficiently to be detected using magnetic resonance (MR) techniques. ^{1}H magnetic resonance spectroscopy studies at ultra-high field have found consistent and reproducible changes in lactate, glutamate, and glucose concentrations[16–18] that result from sensory stimuli. Changes in other metabolites such as glutamine have also been reported.[19] Brain activity has also been shown to lower pH, detectable during

[1]Department of Radiology, University of Iowa, Iowa City, Iowa, USA; [2]Department of Biomedical Engineering, University of Iowa, Iowa City, Iowa, USA; [3]Department of Psychiatry, University of Iowa, Iowa City, Iowa, USA; [4]Department of Neurosurgery, University of Iowa, Iowa City, Iowa, USA and [5]Department of Veterans Affairs Medical Center, Iowa City, USA. Correspondence: Dr VA Magnotta, Department of Radiology, University of Iowa, L311 PBDB, 169 Newton Road, Iowa City, Iowa 52242, USA.
E-mail: vincent-magnotta@uiowa.edu
This study was funded in part by a grant from the Dana Foundation and an Independent Investigator Award from the Brain & Behavior Research Foundation. JAW is supported by the Department of Veterans Affairs (Merit Award), the National Institute of Mental Health (1R01MH085724-01), and the National Heart Lung and Blood Institute (R01HL113863-01). This study was also supported in part by the National Center for Advancing Translational Sciences (U54TR001013).
Received 9 January 2015; revised 8 April 2015; accepted 9 April 2015; published online 13 May 2015

visual cortex activation in humans by ^{31}P magnetic resonance spectroscopy[20,21] and in response to neural activation in mice with an implanted fiberoptic pH sensor.[22] Magnetic resonance spectroscopy techniques have traditionally experienced low spatial and temporal resolution[17,23,24] making it difficult to dynamically measure the metabolic changes that result from neuronal activity. The field of neuroscience would greatly benefit from the ability to noninvasively image local metabolic changes with high spatial and temporal resolution as a more direct approach to study brain function.

The MR imaging techniques that are sensitive to proton exchange have been gaining popularity. These imaging techniques include chemical exchange saturation transfer and T_1 relaxation in the rotating frame ($T_{1\rho}$). Proton exchange between bulk water and amide, hydroxyl, and amine groups of metabolites and proteins are the primary contributors to $T_{1\rho}$ and chemical exchange saturation transfer contrast in biologic tissue.[25] $T_{1\rho}$ imaging applies a low amplitude spin-lock pulse, which makes the sequence sensitive to proton exchange between metabolites and bulk water that occurs near the frequency of the applied spin-lock pulse. It has been previously shown that the $T_{1\rho}$ relaxation time is sensitive to metabolism including pH[21,25,26] as well as glucose and glutamate concentrations.[27] Functional $T_{1\rho}$ mapping has recently been shown to exhibit a response in the visual cortex resulting from stimulation using a flashing checkerboard both in humans[21,28] and in animals.[27] Work to date has shown that the technique is relatively immune to changes in blood oxygenation[21] and that the signal exists even when minimizing the vascular component using contrast agents[27] or saturation pulses.[20] Further characterization of the functional $T_{1\rho}$ response temporal dynamics may provide additional evidence that the signal arises predominantly from metabolic changes rather than the vascular response.

In this study, we compared the temporal dynamics of three functional imaging techniques ($T_{1\rho}$ mapping, BOLD, and ASL) using retinotopic eccentricity mapping. The three functional imaging techniques acquired data while subjects viewed an expanding ring stimulus, which induces traveling waves of neural activity in the visual cortex. We calculated the phase maps for eccentricity across the occipital cortex for each functional imaging method and compared their temporal responses. Eccentricity mapping provides the ability to measure subtle response timing differences across the entire visual cortex. We hypothesized that the functional $T_{1\rho}$ response in the visual cortex would precede the hemodynamic response measured by functional imaging using BOLD and ASL contrast. This would provide strong evidence that the functional $T_{1\rho}$ response is driven by local metabolic and pH changes evoked by neural activity that precede the hemodynamic response.

MATERIALS AND METHODS

Subjects

Five subjects (three men and two women, 29 to 33 years of age) were enrolled into an MR imaging study that included the acquisition of both anatomic (T_1-weighted) and functional ($T_{1\rho}$, BOLD, and ASL) images. All subjects had normal or corrected-to-normal vision. Signed informed consent was obtained before beginning the study in accordance with the Institutional Review Board at the University of Iowa and all experiments were performed in accordance with the guidelines outlined in the Belmont Report.

Data Acquisition

Magnetic resonance images were obtained on a 3.0-T Siemens TIM Trio scanner (Siemens Medical Solutions, Erlangen, Germany) using a 12-channel head coil. For cortical surface reconstruction, high-resolution anatomic T_1-weighted images were acquired using a coronal three-dimensional MP-RAGE sequence (repetition time (TR) = 2,530 ms, echo time (TE) = 2.8 ms, inversion time TI = 909 ms, flip angle = 10°, field of view = 256 × 256 × 256 mm, matrix size = 256 × 256 × 256, bandwidth = 180 Hz/pixel). The BOLD imaging was performed using a T_2*-weighted echo-planar gradient-echo sequence (TR = 2,500 ms, TE = 30 ms, flip angle = 90°, field of view = 220 × 220 mm, matrix size = 64 × 64, bandwidth = 2004 Hz/pixel, number of slices = 31, and slice thickness/gap = 4.0/1.0 mm). The BOLD acquisition provided whole brain coverage in the slice direction. A run of BOLD imaging collected 124 frames of data for an imaging time of 310 seconds per run. Functional $T_{1\rho}$ mapping was performed using an echo-planar spin-echo sequence with an additional $T_{1\rho}$ spin-lock encoding pulse, which has been previously described.[20,21,28,29] For this particular implementation, sequence parameters were TR = 2,500 ms, TE = 12ms, field of view = 220 × 220 mm, matrix size = 64 × 64, bandwidth = 1,954 Hz/pixel, number of slices = 15, and slice thickness/gap = 4.0/1.0 mm. Two spin-lock pulses were used (10 and 40ms) with a spin-lock frequency of 290 Hz. Fat saturation and spin-lock pulses were played out for each slice of the echo-planar imaging sequence, effectively reducing the TR for application of the $T_{1\rho}$ pulse. The $T_{1\rho}$ encoding block consisted of two nonselective 90° pulses separated with a pair of low amplitude spin locking pulses with opposite phase. Crusher gradients were used to destroy any residual magnetization after the $T_{1\rho}$ encoding period. This was followed by a traditional echo-planar imaging sequence with a single-shot readout. This sequence was repeated for each slice of the 15-slice acquisition. After all slices were acquired, the sequence was repeated with a different spin-lock duration. The spin-lock pulse was alternated between 10 and 40 ms durations for each imaging frame. The $T_{1\rho}$ imaging sequence had limited spatial coverage in the slice direction and the imaging slab was centered on the occipital cortex. A total of 124 frames (i.e., 62 frames for each spin-lock duration) were collected in a run of functional $T_{1\rho}$ mapping for a run time of 310 seconds. Pulsed ASL (PICORE Q2T) images were collected by alternating between tag and control images (TR = 2,500 ms, TE = 15 ms, inversion time 1/2 TI_1/TI_2 = 700/1,602 ms, field of view = 220 × 220 mm, matrix size = 64 × 64, number of slices = 12, and slice thickness/gap = 4/1 mm). Similar to the $T_{1\rho}$ imaging sequence, the imaging slab was centered on the visual cortex due to the limited coverage in the slice direction. The ASL acquisition collected 126 pairs of images as well as an M_0 image for a run duration of 318 seconds. Two runs of the ASL and $T_{1\rho}$ measurements were obtained to generate the same number of independent samples for each modality. Three-dimensional shimming was performed for all functional scans using the automatic shimming routine available on the scanner.

Visual Stimulation

Eccentricity mapping was performed using standard expanding-ring stimuli that induce traveling waves of neural activity in the visual cortex.[30–32] For retinotopic mapping of the visual field, the visual stimuli give spatiotemporally localized neural response in primary visual cortex. Eccentricity mapping was performed using an expanding-ring checkerboard presented with a 50-second period (0.02 Hz) for each of three functional modalities (Figure 1A). Six cycles of the expanding-ring stimulus were presented during each functional imaging run. When the ring reached the maximum eccentricity, it wrapped around to the minimum eccentricity. A temporal period of 50 seconds for eccentricity stimulation allowed the signal to return to baseline before subsequent activations. The stimulus patterns were based on a radial high-contrast black and white checkerboard flickering at 8 Hz to maximally stimulate primary visual cortex and generally induce BOLD signal change on the order of 1% to 5%. The stimulus was presented on a screen of width 40 cm, height 30 cm, and a distance of approximately 80 cm from the subject's eye. Subjects viewed the screen through a mirror attached to the head coil. A deep-red colored circle was shown in the center of the stimulus. Subjects were asked to press a button on a fiber optic response system (Lumin LP-400, Cedrus Corporation, San Pedro, CA, USA) when the deep-red colored circle changed to bright red, which occurred at random times. This was performed to ensure that the subjects maintained fixation on the center throughout the stimulus presentation. A trigger pulse generated by the scanner was used to initiate the stimulus presentation and six dummy scans (6 × TR = 15 seconds) were collected at the beginning of each run to reach steady-state magnetization before initiating the eccentricity mapping stimulus. The stimuli were presented to the subjects using MATLAB (The MathWorks, Inc., Natick, MA, USA) and the Psychophysics Toolbox.[33,34]

Image Analysis

The cortical surface of each subject was reconstructed from the high-resolution T_1-weighted images using Freesurfer.[35,36] The FreeSurfer pipeline first performs tissue classification before separating the hemispheres

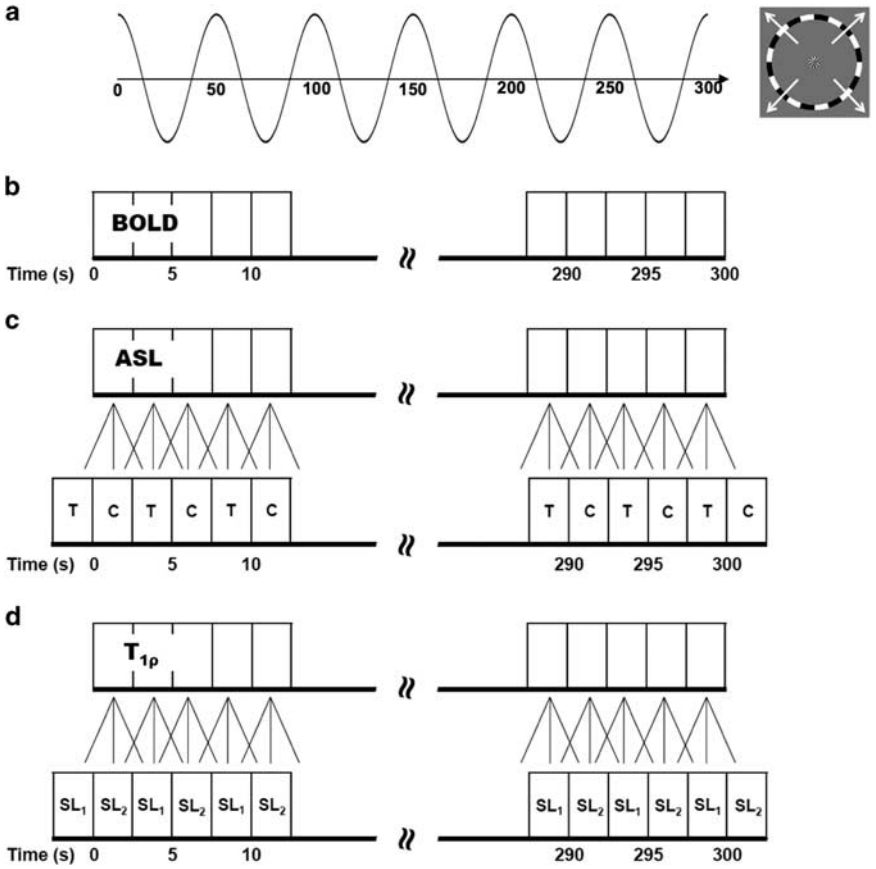

Figure 1. Expanding-ring visual stimulus paradigm used for the functional imaging experiments. (**A**) Traveling wave eccentricity mapping paradigm used to activate the visual cortex. The phase of the sinusoidal wave varies as a function of distance from the center of the visual field. (**B**) Blood oxygenation level-dependent (BOLD) imaging experiment data acquisition. (**C**) The arterial spin labeling (ASL) imaging experiment calculated difference images using sliding window with linear interpolation to estimate C (control) and T (tag) images for each repetition time (TR). (**D**) $T_{1\rho}$ imaging experiment estimated the $T_{1\rho}$ relaxation times using a mono-exponential fit along with sliding window and linear interpolation to estimate the SL_1 (spin-lock duration time = 10 ms) and SL_2 (spin-lock duration time = 40 ms) spin-lock images for each TR.

and generating a separate surface for each hemisphere. The occipital lobe was flattened by cutting the inflated surface along the calcarine fissure. Results from this study are shown both on the inflated surface and on the flattened occipital cortex.

All functional imaging data were analyzed using a combination of AFNI/SUMA (1996[37]) and additional custom-written MATLAB software. Preprocessing for all the BOLD functional data included outlier detection, slice timing correction, and three-dimensional motion correction. The BOLD time series data (Figure 1B) were detrended using a third-order polynomial and normalized to percent signal change. Preprocessing of the ASL and functional $T_{1\rho}$ mapping data was initiated by performing motion correction of the time series data using a mutual information metric and a rigid body transformation. After motion correction, the ASL and functional $T_{1\rho}$ mapping data were analyzed using different MATLAB scripts. For the ASL data, control–tag difference images were calculated using temporal interpolation and sliding window subtraction (Figure 1C) to reduce BOLD signal contamination of the cerebral blood flow (CBF) time course.[38] The resulting time series had a temporal resolution equal to the TR time for the imaging sequence. For the $T_{1\rho}$ mapping data, the approach described in Johnson *et al*[29] employing sliding window interpolation was used (Figure 1D). Briefly, this procedure estimates a $T_{1\rho}$ map using a mono-exponential fit, $S = S_0 e^{-TSL/T1\rho}$, at each TR. The fit is performed using the spin-lock image collected at one time point (e.g., 10 ms) and the average of the two temporally neighboring spin-lock images (e.g., 40 ms). This is then repeated for each image in the time series, resulting in a temporal sampling of the $T_{1\rho}$ maps equal to the TR. The use of multiple images to estimate perfusion and $T_{1\rho}$ relaxation times eliminates baseline fluctuations in the signal and thus no baseline modeling was included in the analysis of the ASL and $T_{1\rho}$ data. For the functional $T_{1\rho}$ mapping, the top and bottom two slices were eliminated from the analysis since the magnetization was reaching a steady state after switching the spin-lock duration.[29]

The voxelwise phase and amplitude of neuronal responses for all functional modalities were estimated by taking the Fourier transform of the time series and measuring the response at the stimulation frequency (0.02 Hz).

Image alignment between the functional activation maps and *T*1-weighted anatomic scan was performed using a rigid body registration. The resulting transform was used to resample the functional activation maps (phase and coherence) to 1.0 mm isotropic resolution, matching the anatomic image resolution and allowing the phase maps to be overlaid on the cortical surface. The phase data were then smoothed with a Gaussian kernel of 6 mm FWHM along the cortical surface. The phase maps were color coded between 0 (red) and 2π (green). For each voxel, we calculated an *F* ratio and the corresponding *P*-values by dividing the squared amplitude of the response at the fundamental stimulus frequency (0.02 Hz) with the average squared amplitude at all other frequencies except the signal at the DC component frequency. For each subject, the statistical map of BOLD eccentricity was thresholded ($P < 0.01$, FDR corrected) and a region of interest (ROI) was defined by significantly activated voxels of the thresholded eccentricity map. The statistical maps of ASL and $T_{1\rho}$ eccentricity were similarly thresholded but at a lower significance level than BOLD ($P < 0.05$, FDR corrected) because of the lower SNR of these techniques. The BOLD-defined ROI was used to compare the phase maps between modalities (BOLD-ASL, BOLD-$T_{1\rho}$, and ASL-$T_{1\rho}$). The resulting phase differences were converted to seconds for display and further analysis.

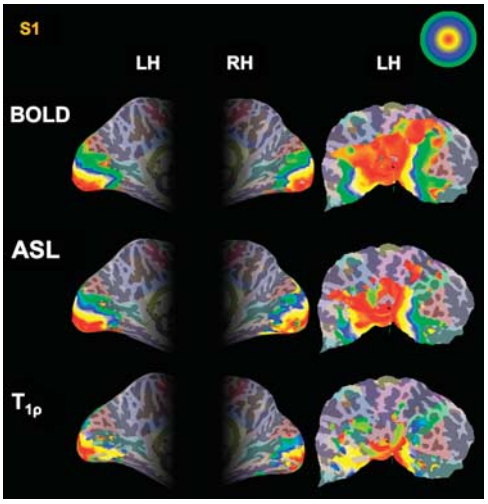

Figure 2. Eccentricity phase maps of blood oxygenation level-dependent (BOLD), arterial spin labeling (ASL), and $T_{1\rho}$ response to the expanding-ring stimulus on the left and right inflated hemisphere, and the left flattened brain surface for single subject (S1). The color scale indicates the raw phase value between 0 and 2π for eccentricity map. The red color indicates regions corresponding to the center of field of view, while the green color regions correspond to the outer eccentric degrees.

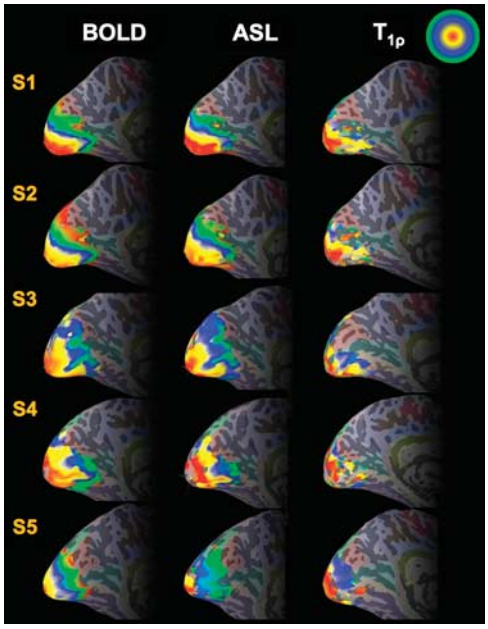

Figure 3. Eccentricity phase maps of blood oxygenation level-dependent (BOLD), arterial spin labeling (ASL), and $T_{1\rho}$ response to the expanding-ring stimulus on the left inflated hemisphere as shown in Figure 2 for all five participants in the study (S1 to S5).

An ROI analysis was performed to compare the mean time course of the functional response across all three modalities (functional $T_{1\rho}$ mapping, BOLD, and ASL). A $2\times2\times2$ voxel ROI was placed in the primary visual cortex (V1) where all three modalities had a statistically significant response. The time courses from within the ROI were then individually normalized between ±1 using the minimum and maximum values for each modality. The time series for each modality were also collapsed (excluding the first and last cycle) to generate the mean response over a single period. Quantitative analysis consisted of computing the mean phase lag and the time to peak (TTP) of the functional imaging responses. The phase lag within the ROI for each modality was computed, which estimates the temporal delay of the fMRI responses relative to the beginning of the time series. To compute the TTP, a gamma-variate function ($\gamma = a\times x\times e^{-bx}+c$) was used to fit to the mean response over a single period. The TTP was defined as $1/b$ from the fitted lineshape. The phase lag and the TTP values were statistically compared using a two-way ANOVA followed by Tukey's *post hoc* test. Statistical significance was accepted for $P < 0.05$.

RESULTS

Figure 2 shows the phase map generated from the expanding-ring eccentricity mapping study for functional $T_{1\rho}$ mapping, BOLD, and ASL imaging on the left and right hemisphere inflated surfaces as well as on the flattened left cortical surface for a single subject (Subject #1 = S1). Only voxels that had met the statistical threshold as specified in the Materials and methods section for each modality are shown in the figure. The color scale (upper right corner of Figure 2) indicates the phase value between 0 (red) and 2π (green) for eccentricity mapping. The eccentricity maps show a systematic increase in phase (red to green) originating from the occipital pole toward more anterior regions across all three modalities. Figure 3 shows phase maps for $T_{1\rho}$, BOLD, and ASL imaging resulting from the expanding-ring eccentricity mapping on the left hemisphere inflated cortical surface for all five subjects (Subject #1 = S1, Subject #2 = S2, Subject #3 = S3, Subject #4 = S4, and Subject #5 = S5). The responses from BOLD and ASL imaging show a robust activation while the functional $T_{1\rho}$ mapping response tends to be weaker.

Figure 4A shows the eccentricity phase maps for functional $T_{1\rho}$ mapping, BOLD, and ASL overlaid on sagittal (upper) and axial (lower) echo-planar images for a representative subject (S1). Figure 4B shows the subtracted time delay maps (BOLD-ASL, BOLD-$T_{1\rho}$, and ASL-$T_{1\rho}$) within the region that had a significant BOLD response. The difference image (Figure 4B) largely show a faster response (white-to-red) in the functional $T_{1\rho}$ mapping as compared with BOLD and ASL imaging.

A time series plot for a single representative subject is shown in Figure 4C within the ROI defined in the visual cortex. The location of the ROI is shown in red in Figure 4A. The mean value is the solid line and the shaded area in the same color represents the standard deviation of the values contained within the ROI as shown in Figure 4C. The collapsed time series data representing the mean response for one period of the eccentricity mapping is shown in Figure 4D. This figure shows the mean time series as a solid line and the standard deviation in the shaded area of the same color. These plots suggest that the functional $T_{1\rho}$ response occurs before the hemodynamic response seen in BOLD and ASL imaging. Across all five subjects in the study the phase lag in the $T_{1\rho}$ response occurred on average 1.3 and 3.0 seconds faster than the ASL and BOLD responses, respectively (Table 1). In addition, the average TTP for the five subjects also occurred earlier for functional $T_{1\rho}$ mapping as compared with ASL and BOLD imaging (1.8 and 3.4 seconds, respectively). All of these differences were statistically significant ($P < 0.05$).

DISCUSSION

In this study, retinotopic eccentricity mapping was performed using an expanding-ring visual stimulation with a 50-second period was used to compare the temporal response between functional $T_{1\rho}$ mapping, BOLD, and ASL imaging. The occipital cortex was used as a model system for this study since it is relatively easy to perform such subtle manipulations of the stimuli for fine mapping of the visual cortex. Our results showed that functional $T_{1\rho}$ mapping has a faster temporal response as compared with BOLD and ASL. On average, the $T_{1\rho}$ signal preceded the BOLD signal by 3.0 seconds and the ASL signal by 1.3 seconds. These data suggest that the functional $T_{1\rho}$ mapping signal is largely independent of the vascular response. Instead, the

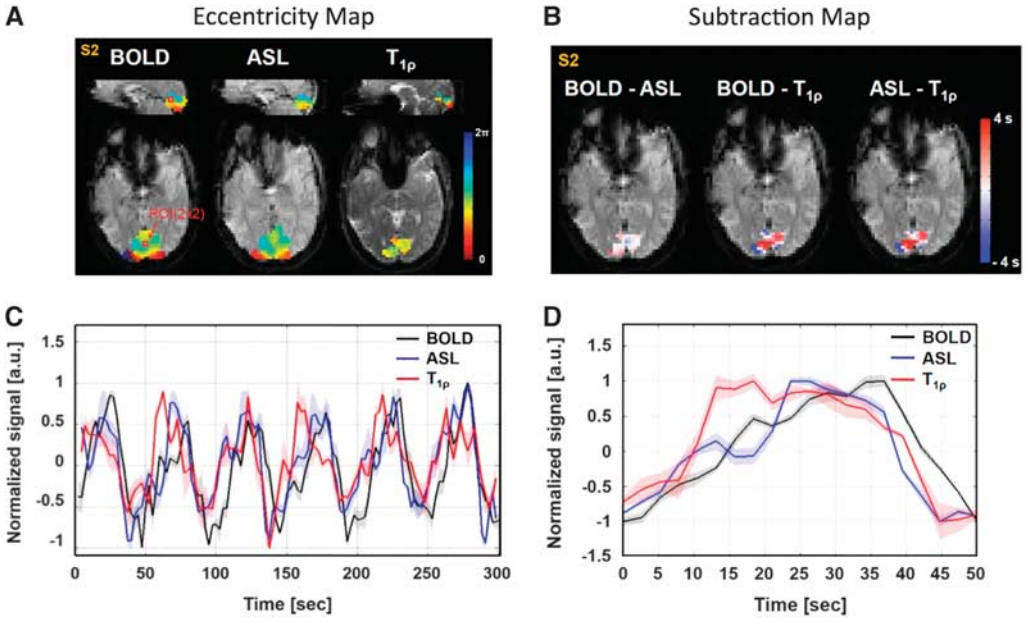

Figure 4. Eccentricity phase maps and normalized signal changes of blood oxygenation level-dependent (BOLD), arterial spin labeling (ASL), and $T_{1\rho}$ response for a representative subject (S1). (**A**) Phase maps of the BOLD, ASL, and $T_{1\rho}$ responses overlaid on the sagittal (upper) and axial (lower) functional images. (**B**) Time delay subtraction images between the BOLD and ASL (left), BOLD and $T_{1\rho}$ (middle), and ASL and $T_{1\rho}$ (right) phase maps. (**C**) Mean time courses obtained from the ROI within the primary visual cortex shown as a black square in (**A**). The data for BOLD (black line), ASL (blue line), and $T_{1\rho}$ (red line) have been normalized to ± 1. (**D**) Averaged signal changes of the BOLD (black line), ASL (blue line), and $T_{1\rho}$ (red line) time courses for one period. Error bars depict the standard deviation.

Table 1. Difference in the phase lag and time to peak (TTP) in the response between BOLD, ASL, and functional $T_{1\rho}$ mapping

Subject	*Phase lag*		*TTP*	
	BOLD-$T_{1\rho}$ (seconds)	*ASL-$T_{1\rho}$ (seconds)*	*BOLD-$T_{1\rho}$ (seconds)*	*ASL-$T_{1\rho}$ (seconds)*
S1	2.7	0.2	5.1	1.2
S2	2.9	2.0	6.2	1.4
S3	2.3	1.5	1.4	2.4
S4	3.8	0.9	0.3	-0.2
S5	3.1	2.0	4.2	4.2
Mean ± s.d.	3.0 ± 0.6^a	1.3 ± 0.8^a	3.4 ± 2.5^a	1.8 ± 1.6^a

Abbreviations: ASL, arterial spin labeling; BOLD, blood oxygenation level-dependent. [a]Statistically significant ($P < 0.05$).

signal may be the result of metabolic changes such as decreased pH or glucose concentrations that would generate an increase in the measured $T_{1\rho}$ relaxation times. Jin and Kim[27] have also found that $T_{1\rho}$ signal from tissue is faster than the BOLD and cerebral blood volume response measured in the cat visual cortex. Their findings are in good agreement with the data obtained in this study. It has been suggested that the hemodynamic response is increasingly delayed as the blood progresses toward larger draining veins, with delays ranging between 2 seconds in the parenchyma to 14 seconds in the large draining veins.[4,5] We have previously shown that the $T_{1\rho}$ changes are independent of blood oxygenation.[21] More recently, we as well as others have shown that $>70\%$ of the functional $T_{1\rho}$ mapping signal exists even when the signal from inflowing blood is nulled, which provides further evidence that the signal is metabolic in nature and not the result of blood flow changes.[20,27] In addition, the results from this study found that the hemodynamic response from ASL imaging occurred approximately 2 seconds faster than BOLD within the visual cortex. These data are consistent with values previously reported in the literature.[10]

We found that the number of significantly activated voxels was greater in BOLD and ASL imaging as compared with functional $T_{1\rho}$ mapping. This was not tested statistically, but is consistent with our previous published work.[20,29] Recently, Heo *et al*[20] assessed the number of activated voxels for each of three stimulations frequencies (1, 4, and 7 Hz) using both BOLD and functional $T_{1\rho}$ mapping. Heo *et al*[20] found that approximately 50 to 100 times more voxels were activated in the visual cortex for BOLD imaging as compared with functional $T_{1\rho}$ mapping at the same statistical threshold ($P < 0.05$, corrected). It should be noted that in the present study we used two different statistical thresholds, $P < 0.01$ for BOLD imaging and $P < 0.05$ for ASL and functional $T_{1\rho}$ mapping. It is well known that the BOLD signal is primarily caused by oxygenation and volume changes in veins, which can spread the fMRI-detected area to regions where there are no neuronal activation, whereas ASL is more closely associated with the capillary bed.[6,9,38] While the $T_{1\rho}$ activation area was contained mostly within the BOLD and ASL activation area, it was significantly smaller. The differences in the spatial extent of the functional response can be explained by both the different mechanisms driving the signal for each of the imaging method as well as the respective contrast-to-noise ratio for each method. Using receiver operator characteristic analysis, previous studies reported that ASL shows distinctive noise properties compared with BOLD contrast because ASL image series are generated by surround subtraction of temporally adjacent control and tag images, resulting in the even distribution of noise power spectrum and spatial coherence.[39] For ASL data, the surround subtraction method (Figure 1C) was used to reduce BOLD signal contamination of the CBF time course, and it is also advantageous to match the timing of the control and tag images. However, this method does result in some temporal smoothing of the data. Even with the use of the temporal interpolation approach for both ASL and functional $T_{1\rho}$ mapping, we still found that the ASL response occurred before the BOLD response and the $T_{1\rho}$ response occurred faster than ASL. It should be noted that we assessed the positive BOLD response resulting from increased oxygenated

hemoglobin. Several prior studies have shown that the initial undershoot of the BOLD response that occurs before the increased blood flow response is faster and more localized to the region of activation.[40,41] This initial undershoot is a weak signal that is not consistently observed in BOLD imaging studies conducted at 1.5 and 3 T, which is why this technique has not been widely adopted for functional imaging. In future studies, it would be interesting to compare the location of brain activity identified by function $T_{1\rho}$ mapping with the initial dip in the BOLD response.

Neural activity and CBF are closely coupled.[42] Increases in oxygen and glucose consumption during neural activity are followed by an increase in CBF. In addition, the CBF is controlled by feedback mechanisms, which are correlated with the concentration of metabolic byproducts such as nitric oxide, adenosine, carbon dioxide, and arachidonic acid metabolites.[42–45] Prior studies have shown that local acidosis may alter blood flow by depolarizing the vascular smooth muscle cells, which trigger vasodilation.[42] Consequently, activity-evoked acidosis may be a key mechanism underlying neurovascular coupling. Nevertheless, current functional imaging paradigms are limited by their dependence on blood flow, blood volume, and the vascular anatomy, which limits their temporal and spatial resolution. However, functional $T_{1\rho}$ mapping could be a more direct and precise method of imaging brain functions because local changes in metabolism drive the vascular response. Several possible sources for changes in $T_{1\rho}$ relaxation times with brain activity include sensitivity to pH,[21,25–27] glutamate, and glucose.[27] In addition, we have not yet optimized the amplitude of the spin-lock pulse used. For application to human imaging, we have been limited by subject heating to amplitudes $< 1{,}000$ Hz. Future studies are needed to determine the metabolic changes that occur with brain function that drive the functional $T_{1\rho}$ response and the optimal spin-lock amplitude for measuring the metabolic changes of interest. Finally, it is also possible that metabolic changes could also influence BOLD and ASL signals through changes in T_1 relaxation rates that have not been realized due to the noise or mistaken as noise in the functional imaging signals. For example, Shemesh *et al*[46] found significant changes in the T_1 relaxation times in various metabolites including lactate and creatine in a rat ischemia model at 21.1 T. The magnitude of this effect at clinical fields strengths resulting from brain function is presently unknown.

In conclusion, we performed eccentric mapping of the human brain at 3 T using the expanding-ring stimulus to assess the temporal response of functional $T_{1\rho}$ mapping relative to BOLD and ASL. Our study suggests that functional $T_{1\rho}$ mapping signal has a faster temporal response as compared with the hemodynamic response. This is further evidence that the $T_{1\rho}$ signal is driven in part by nonvascular mechanisms at clinical field strength (3.0 T). Therefore, $T_{1\rho}$ imaging may be useful to map neural activation more precisely than blood flow-dependent methods.

AUTHOR CONTRIBUTIONS

H-YH designed and conducted experiments, performed image analysis, prepared original manuscript and figures. JAW and VAM participated in experimental design and manuscript preparation and review. CPJ and DRT participated in pulse sequence development as well as in manuscript preparation and review.

DISCLOSURE/CONFLICT OF INTEREST

The authors declare no conflict of interest.

REFERENCES

1 Boxerman JL, Bandettini PA, Kwong KK, Baker JR, Davis TL, Rosen BR *et al.* The intravascular contribution to fMRI signal change: Monte Carlo modeling and diffusion-weighted studies in vivo. *Magn Reson Med* 1995; **34**: 4–10.
2 Buxton RB, Wong EC, Frank LR. Dynamics of blood flow and oxygenation changes during brain activation: the balloon model. *Magn Reson Med* 1998; **39**: 855–864.
3 Ugurbil K, Toth L, Kim DS. How accurate is magnetic resonance imaging of brain function? *Trends Neurosci* 2003; **26**: 108–114.
4 Lee AT, Glover GH, Meyer CH. Discrimination of large venous vessels in time-course spiral blood-oxygen-level-dependent magnetic-resonance functional neuroimaging. *Magn Reson Med* 1995; **33**: 745–754.
5 Saad ZS, Ropella KM, Cox RW, DeYoe EA. Analysis and use of FMRI response delays. *Hum Brain Mapp* 2001; **13**: 74–93.
6 Detre JA, Leigh JS, Williams DS, Koretsky AP. Perfusion imaging. *Magn Reson Med* 1992; **23**: 37–45.
7 Lu H, Golay X, Pekar JJ, Van Zijl PC. Functional magnetic resonance imaging based on changes in vascular space occupancy. *Magn Reson Med* 2003; **50**: 263–274.
8 Mandeville JB, Marota JJ, Kosofsky BE, Keltner JR, Weissleder R, Rosen BR *et al.* Dynamic functional imaging of relative cerebral blood volume during rat forepaw stimulation. *Magn Reson Med* 1998; **39**: 615–624.
9 Silva AC, Williams DS, Koretsky AP. Evidence for the exchange of arterial spin-labeled water with tissue water in rat brain from diffusion-sensitized measurements of perfusion. *Magn Reson Med* 1997; **38**: 232–237.
10 Cavusoglu M, Bartels A, Yesilyurt B, Uludağ K. Retinotopic maps and hemodynamic delays in the human visual cortex measured using arterial spin labeling. *NeuroImage* 2012; **59**: 4044–4054.
11 Sheth SA, Nemoto M, Guiou M, Walker M, Pouratian N, Hageman N *et al.* Columnar specificity of microvascular oxygenation and volume responses: implications for functional brain mapping. *J Neurosci* 2004; **24**: 634–641.
12 Mandeville JB, Marota JJ, Ayata C, Zaharchuk G, Moskowitz MA, Rosen BR *et al.* Evidence of a cerebrovascular postarteriole windkessel with delayed compliance. *J Cereb Blood Flow Metab* 1999; **19**: 679–689.
13 Silva AC, Koretsky AP, Duyn JH. Functional MRI impulse response for BOLD and CBV contrast in rat somatosensory cortex. *Magn Reson Med* 2007; **57**: 1110–1118.
14 Zong X, Kim T, Kim SG. Contributions of dynamic venous blood volume versus oxygenation level changes to BOLD fMRI. *NeuroImage* 2012; **60**: 2238–2246.
15 Cipolla MJ *The cerebral circulation*. Morgan & Claypool Life Sciences: San Rafael, CA, 2009.
16 Lin Y, Stephenson MC, Xin L, Napolitano A, Morris PG. Investigating the metabolic changes due to visual stimulation using functional proton magnetic resonance spectroscopy at 7 T. *J Cereb Blood Flow Metab* 2012; **32**: 1484–1495.
17 Mangia S, Tkac I, Gruetter R, Van de Moortele PF, Maraviglia B, Ugurbil K. Sustained neuronal activation raises oxidative metabolism to a new steady-state level: evidence from 1H NMR spectroscopy in the human visual cortex. *J Cereb Blood Flow Metab* 2007; **27**: 1055–1063.
18 Schaller B, Mekle R, Xin L, Kunz N, Gruetter R. Net increase of lactate and glutamate concentration in activated human visual cortex detected with magnetic resonance spectroscopy at 7 tesla. *J Neurosci Res* 2013; **91**: 1076–1083.
19 Ramadan S, Lin A, Stanwell P. Glutamate and glutamine: a review of in vivo MRS in the human brain. *NMR Biomed* 2013; **26**: 1630–1646.
20 Heo HY, Wemmie J, Thedens D, Magnotta VA. Evaluation of activity-dependent functional pH and T1rho response in the visual cortex. *NeuroImage* 2014; **95**: 336–343.
21 Magnotta VA, Heo HY, Dlouhy BJ, Dahdaleh NS, Follmer RL, Thedens DR *et al.* Detecting activity-evoked pH changes in human brain. *Proc Natl Acad Sci USA* 2012; **109**: 8270–8273.
22 Ziemann AE, Schnizler MK, Albert GW, Severson MA, Howard MA, 3rd, Welsh MJ *et al.* Seizure termination by acidosis depends on ASIC1a. *Nat Neurosci* 2008; **11**: 816–822.
23 Xu S, Yang J, Li CQ, Zhu W, Shen J. Metabolic alterations in focally activated primary somatosensory cortex of alpha-chloralose-anesthetized rats measured by 1H MRS at 11.7 T. *NeuroImage* 2005; **28**: 401–409.
24 Hyder F, Chase JR, Behar KL, Mason GF, Siddeek M, Rothman DL *et al.* Increased tricarboxylic acid cycle flux in rat brain during forepaw stimulation detected with 1H[13C]NMR. *Proc Natl Acad Sci USA* 1996; **93**: 7612–7617.
25 Jin T, Autio J, Obata T, Kim SG. Spin-locking versus chemical exchange saturation transfer MRI for investigating chemical exchange process between water and labile metabolite protons. *Magn Reson Med* 2011; **65**: 1448–1460.
26 Kettunen MI, Grohn OH, Silvennoinen MJ, Penttonen M, Kauppinen RA. Effects of intracellular pH, blood, and tissue oxygen tension on T1rho relaxation in rat brain. *Magn Reson Med* 2002; **48**: 470–477.
27 Jin T, Kim SG. Characterization of non-hemodynamic functional signal measured by spin-lock fMRI. *NeuroImage* 2013; **78**: 385–395.

28 Magnotta VA, Johnson CP, Follmer R, Wemmie JA. Functional t1rho imaging in panic disorder. *Biol Psychiatry* 2014; **75**: 884–891.
29 Johnson CP, Heo HY, Thedens DR, Wemmie JA, Magnotta VA. Rapid acquisition strategy for functional T1rho mapping of the brain. *Magn Reson Med* 2014; **32**: 1067–1077.
30 Engel SA, Glover GH, Wandell BA. Retinotopic organization in human visual cortex and the spatial precision of functional MRI. *Cereb Cortex* 1997; **7**: 181–192.
31 Engel SA, Rumelhart DE, Wandell BA, Lee AT, Glover GH, Chichilnisky EJ *et al.* fMRI of human visual cortex. *Nature* 1994; **369**: 525.
32 Sereno MI, Dale AM, Reppas JB, Kwong KK, Belliveau JW, Brady TJ *et al.* Borders of multiple visual areas in humans revealed by functional magnetic resonance imaging. *Science* 1995; **268**: 889–893.
33 Brainard DH. The Psychophysics Toolbox. *Spat Vis* 1997; **10**: 433–436.
34 Pelli DG. The VideoToolbox software for visual psychophysics: transforming numbers into movies. *Spat Vis* 1997; **10**: 437–442.
35 Dale AM, Fischl B, Sereno MI. Cortical surface-based analysis. I. Segmentation and surface reconstruction. *NeuroImage* 1999; **9**: 179–194.
36 Fischl B, Sereno MI, Dale AM. Cortical surface-based analysis. II: Inflation, flattening, and a surface-based coordinate system. *NeuroImage* 1999; **9**: 195–207.
37 Cox RW. AFNI: software for analysis and visualization of functional magnetic resonance neuroimages. *Comput Biomed Res* 1996; **29**: 162–173.
38 Wong EC, Buxton RB, Frank LR. Quantitative imaging of perfusion using a single subtraction (QUIPSS and QUIPSS II). *Magn Reson Med* 1998; **39**: 702–708.
39 Wang J, Wang Z, Aguirre GK, Detre JA. To smooth or not to smooth? ROC analysis of perfusion fMRI data. *Magn Reson Med* 2005; **23**: 75–81.
40 Duong TQ, Kim DS, Ugurbil K, Kim SG. Spatiotemporal dynamics of the BOLD fMRI signals: toward mapping submillimeter cortical columns using the early negative response. *Magn Reson Med* 2000; **44**: 231–242.
41 Kim DS, Duong TQ, Kim SG. High-resolution mapping of iso-orientation columns by fMRI. *Nat Neurosci* 2000; **3**: 164–169.
42 Kety SS, Schmidt CF. The effects of altered arterial tensions of carbon dioxide and oxygen on cerebral blood flow and cerebral oxygen consumption of normal young men. *J Clin Invest* 1948; **27**: 484–492.
43 Dirnagl U, Lindauer U, Villringer A. Role of nitric oxide in the coupling of cerebral blood flow to neuronal activation in rats. *Neurosci Lett* 1993; **149**: 43–46.
44 Harder DR, Alkayed NJ, Lange AR, Gebremedhin D, Roman RJ. Functional hyperemia in the brain: hypothesis for astrocyte-derived vasodilator metabolites. *Stroke* 1998; **29**: 229–234.
45 Ko KR, Ngai AC, Winn HR. Role of adenosine in regulation of regional cerebral blood flow in sensory cortex. *Am J Physiol* 1990; **259**: H1703–H1708.
46 Shemesh N, Rosenberg JT, Dumez JN, Grant SC, Frydman L. Metabolic T1 dynamics and longitudinal relaxation enhancement in vivo at ultrahigh magnetic fields on ischemia. *J Cereb Blood Flow Metab* 2014; **34**: 1810–1817.